

# Spatiotemporal complexity of a three-species ratio-dependent food chain model

Feng Rao

Received: 29 September 2013 / Accepted: 2 January 2014 / Published online: 29 January 2014  
© Springer Science+Business Media Dordrecht 2014

**Abstract** In this paper, we investigate the complex dynamics of a ratio-dependent spatially extended food chain model. Through a detailed analytical study of the reaction–diffusion model, we obtain some conditions for global stability. On the basis of bifurcation analysis, we present the evolutionary process of pattern formation near the coexistence equilibrium point  $(N^*, P^*, Z^*)$  via numerical simulation. And the sequence cold spots  $\rightarrow$  stripe–spots mixtures  $\rightarrow$  stripes  $\rightarrow$  hot stripe–spots mixtures  $\rightarrow$  hot spots  $\rightarrow$  chaotic wave patterns controlled by parameters  $a_1$  or  $c_1$  in the model are presented. These results indicate that the reaction–diffusion model is an appropriate tool for investigating fundamental mechanism of complex spatiotemporal dynamics.

**Keywords** Food chain model · Stability · Pattern formation · Turing/Hopf bifurcation

## 1 Introduction

Because of the universal existence of prey and predator and their importance in ecology, the dynamical relationship between them has long been, and will continue to be, one of the dominant themes [2].

Prey–predator interaction is one of the basic interspecies relations for ecosystems, and it is also the basic block of more complicated food chain, food web, and biophysical network structures [3]. Complex networks play an important role for describing the organization of biological systems. Evolutionary food web models provide a mechanistic tool to understand how complex ecosystems emerge and how they can persist under changes in their composition and their environment. In particular, the notion of food chain has proven to be very useful to capture the basic properties of “who eats whom” in ecological communities [23]. On ecological food chain, species higher can significantly impact the populations of species below them. And the productivity of food chains is thought to be governed by bottom-up forces, where the populations are resource limited by the lowest-level species [8]. For example, in aquatic ecosystems bottom up control occurs in temperate climate zones. The phytoplankton in the water grow rapidly during the spring when sunlight increases and the water is nutrient-rich from the winter. This growth then provides more food for the zooplankton whose population also increases which in turn provides more food for fish. Food chain models, as one of the most important predator–prey systems, have been extensively studied by many researchers (see, [5, 6, 11–13, 19, 24, 27, 35, 42]), and main interesting results been obtained, including global stability, persistence, the extinction of top predator, structures relevant to chaos, existence, uniqueness and stability of positive periodic solution, and so on.

---

F. Rao (✉)  
College of Sciences, Nanjing University of Technology,  
Nanjing 211816, China  
e-mail: raofeng2002@163.com

In general, a classical food chain model with the non-dimensional form can be written as follows:

$$\begin{cases} \frac{dN}{dt} = Nf(N) - a_1g_1(N, P)P, \\ \frac{dP}{dt} = (b_1g_1(N, P) - c_1)P - a_2g_2(P, Z)Z, \\ \frac{dZ}{dt} = (b_2g_2(P, Z) - c_2)Z, \end{cases} \quad (1)$$

where  $N = N(t)$ ,  $P = P(t)$ , and  $Z = Z(t)$  stand for, respectively, the population densities of prey at lowest level of the food chain, intermediate predator that prey upon  $N$ , and top predator that prey upon  $P$  at time  $t$ . All parameters are positive constants,  $a_1$  and  $a_2$  are the maximum ingestion rates of intermediate predator  $P$  and top predator  $Z$ ;  $b_1$  and  $b_2$  the conversion factors of prey to intermediate predator and intermediate predator to top predator;  $c_1$  and  $c_2$  the mortality rates of the intermediate predator and the top predator, respectively. The function  $f(N)$  represents the density-dependent-specific growth rate of prey in the absence of predator.  $g_i$  ( $i = 1, 2$ ) is the functional response, the prey consumption rate by an average single predator, which obviously increases with the prey consumption rate and can be influenced by the predator density. And  $a_i g_i$  ( $i = 1, 2$ ) is the amount of prey consumed per predator per unit time;  $b_i g_i$  ( $i = 1, 2$ ) the predator production per capita with predation [23].

From a biological perspective, individual organisms are distributed in space and typically interact with the physical environment and other organisms in their spatial neighborhood [7]. The predator–prey system models such a phenomenon: pursuit–evasion—predators pursuing prey and prey escaping the predators [4]. In other words, in nature, there is a tendency that the prey would keep away from predators and the escape velocity of the prey may be taken as proportional to the dispersive velocity of the predators. In the same manner, there is a tendency that the predators would get closer to the prey and the chase velocity of predators may be considered to be proportional to the dispersive velocity of the prey [32,39]. This is often done in terms of diffusion, as movement of individuals may be connected with other things, such as searching for food, escaping high infection risks, and so on [23]. In the first case, individuals tend to diffuse in the direction of lower density of population, where there are more resources. In the second case, to avoid higher infections, individuals may move along

the gradient of infectious individuals [22]. Keeping these in view, predation models are considered where the diffusion of individuals is influenced by intraspecific competition pressures and is affected by different classes [25].

In the above sense, a spatial predator–prey model can be considered as a reaction–diffusion predation model; it has been shown that such models are capable of self-organized pattern formation [18]. Turing [34] in 1952 showed that spatial patterns arise not from inhomogeneity of initial or boundary conditions, but purely from the dynamics of the model, i.e., from the interaction of nonlinear reactions of growth processes and diffusion. In mathematics, pattern formation refers to the process that, by changing a bifurcation parameter, the spatially homogeneous steady states lose stability to spatially inhomogeneous perturbations, and stable inhomogeneous solutions arise [37]. It has been shown that spatiotemporal patterns are very likely to be found in the neighborhood of Turing and Hopf bifurcations. The understanding of patterns and mechanisms of spatial dispersal of interacting species is an issue of significant current interest in conservation biology, ecology, and biochemical reactions [23,25]. In recent years, many studies show that the reaction–diffusion model is an appropriate tool for investigating the fundamental mechanism of complex dynamics [15–17,21,26,29,30,33,41,38,45].

Especially, there has been considerable interest in ratio-dependent food chain model recently. Hsu et al. [11] studied a three-trophic level food chain model with ratio-dependent Michaelis–Menten type functional responses, and pointed out that the model is rich in boundary dynamics and is capable of generating such extinction dynamics. A non-autonomous delayed ratio-dependent food chain model was given in Hou and Li [10], and sufficient and realistic conditions for the global existence of positive periodic solutions for the delayed model were obtained. A non-autonomous ratio-dependent food chain model is permanence, extinction, and ultimate boundedness; and global asymptotic stability under some appropriate conditions was discussed in Zeng [44]. Ko and Ahn [13] investigated a food chain model with ratio-dependent functional response under homogeneous Neumann boundary conditions, and focused on the stability and instability of spatially constant equilibria and formation of spatially non-constant patterns. Peng et al. [29] studied the three-species food chain model

with diffusion and ratio-dependent predation functional response. They analyzed the persistent property of the solution, the stability of the constant positive steady state solution, and the existence and nonexistence of non-constant positive steady state solutions. The diffusive ratio-dependent food chain model was considered by Ko and Ahn in [14] and they provided the sufficient conditions for the existence and nonexistence of coexistence states.

But, to the best of our knowledge, for a reaction–diffusion food chain model with ratio-dependent functional response, research on the evolution process of the spatial pattern formation, the mechanism of pattern formation emergence, seems rare. Based on these discussions above, the main objective of the present paper is to use a type of ratio-dependent food chain model to investigate the spatiotemporal dynamics of three species. And, we focus on the following three-species predation–diffusion model, where predator–prey interactions are nonlinear and are based on ratio-dependent functional responses [11],

$$\begin{cases} \frac{\partial N}{\partial t} = N(1 - N) - \frac{a_1 NP}{N + P} + d_1 \nabla^2 N, \\ \frac{\partial P}{\partial t} = \frac{b_1 NP}{N + P} - c_1 P - \frac{a_2 PZ}{P + Z} + d_2 \nabla^2 P, \\ \frac{\partial Z}{\partial t} = \frac{b_2 PZ}{P + Z} - c_2 Z + d_3 \nabla^2 Z. \end{cases} \quad (2)$$

Note that  $d_1, d_2,$  and  $d_3$  are the diffusion coefficients of the three species,  $\nabla^2 = \partial^2/\partial x^2 + \partial^2/\partial y^2$  the usual Laplacian operator in two-dimensional space, and other parameters are the same definition as those above.

The organization of this paper is as follows. In Sect. 2, we present our main results about the stability and bifurcation analysis of model (2), including boundedness and stability of solutions for the non-spatial and spatial model. Then, by performing a series of numerical simulations, we illustrate the emergence of different patterns of model (2), which is followed by Sect. 3. Finally, we give some conclusions and discussions in Sect. 4.

## 2 Model analysis

Since the state variable  $N, P,$  and  $Z$  of model (2) represent population density, positivity insures that they never become zero, and population always survive, and the state space of model (2) is given by  $R^3_+ = \{(N(t),$

$P(t), Z(t)) \in R^3 : N(t) \geq 0, P(t) \geq 0, Z(t) \geq 0\}$ . The boundedness may be interpreted as a natural restriction to growth as a consequence of limited resources [23].

### 2.1 Dynamics of the non-spatial model (2)

**Theorem 1** *In the absence of diffusion, all the solutions of model (2) with nonnegative initial conditions (that initiate in  $R^3_+$ ) are uniformly bounded for all  $t \geq 0$ .*

*Proof* Let  $(N(t), P(t), Z(t))$  be any solution of the non-spatial model (2) with positive initial conditions. Let us consider that  $W = N + \mu P + \nu Z,$  then

$$\frac{dW}{dt} = \frac{dN}{dt} + \mu \frac{dP}{dt} + \nu \frac{dZ}{dt},$$

where we choose  $\mu = a_1/b_1$  and  $\nu = a_1 a_2 / (b_1 b_2).$  Using Eq. (2), we have

$$\frac{dW}{dt} \leq -\theta(N + P + Z) - (N - 1)^2 - 1,$$

where  $\theta = \min\{1, \mu c_1, \nu c_2\},$  then

$$\frac{dW}{dt} + \theta W \leq 1 - (1 - N)^2.$$

Therefore,

$$\frac{dW}{dt} + \theta W \leq 1.$$

Applying the theory of differential inequality we obtain

$$0 < W < \frac{1 - e^{-\theta t}}{\theta} + W(N(0), P(0), Z(0))e^{-\theta t}.$$

For  $t \rightarrow \infty,$  we have  $0 < W < 1/\theta.$

Hence all the solutions of model (2) in the absence of diffusion that initiate in  $R^3_+$  are confined in the region  $D = \{(N, P, Z) \in R^3_+ : W = 1/\theta + \varepsilon, \text{ for any } \varepsilon > 0\}.$  This proves the theorem.  $\square$

It can be seen that, in the absence of diffusion, model (2) has two nonnegative real equilibrium solutions,

- (i)  $E_1 = \left(\frac{b_1 - a_1(b_1 - c_1)}{b_1}, \frac{(b_1 - a_1(b_1 - c_1))(b_1 - c_1)}{b_1 c_1}, 0\right)$  corresponds to extinction of top predator  $Z$  when  $0 < a_1(b_1 - c_1) < b_1;$
- (ii)  $E^* = (N^*, P^*, Z^*)$  corresponds to coexistence of prey and predators, where

$$N^* = \frac{b_1 b_2 - a_1 b_2 (b_1 - c_1) + a_1 a_2 (b_2 - c_2)}{b_1 b_2},$$

$$P^* = \frac{b_2 (b_1 - c_1) - a_2 (b_2 - c_2)}{b_2 c_1 + a_2 (b_2 - c_2)} N^*,$$

$$Z^* = \frac{b_2 - c_2}{c_2} P^*.$$

Noting that the conditions ensuring the positiveness of  $N^*$ ,  $P^*$ , and  $Z^*$  are  $0 < a_1 b_1 (b_1 - c_1) < b_1 b_2 + a_1 a_2 (b_2 - c_2)$  and  $0 < a_2 (b_2 - c_2) < b_2 (b_1 - c_1)$ . The Jacobian matrix  $\mathbf{J}(N, P, Z)$  at any point  $(N, P, Z)$  is given by

$$\mathbf{J}(N, P, Z) = \begin{pmatrix} 1 - 2N - \frac{a_1 P^2}{(N+P)^2} & -\frac{a_1 N^2}{(N+P)^2} & 0 \\ \frac{b_1 P^2}{(N+P)^2} & \frac{b_1 N^2}{(N+P)^2} - c_1 - \frac{a_2 Z^2}{(P+Z)^2} & -\frac{a_2 P^2}{(P+Z)^2} \\ 0 & \frac{b_2 Z^2}{(P+Z)^2} & \frac{b_2 P^2}{(P+Z)^2} - c_2 \end{pmatrix}.$$

**Theorem 2** *The top predator-free equilibrium point  $E_1 = (b_1 - a_1(b_1 - c_1))/b_1, (b_1 - a_1(b_1 - c_1))(b_1 - c_1)/(b_1 c_1), 0$  is stable if  $b_1 c_1 (b_1 - c_1) > a_1 (b_1^2 - c_1^2) - b_1^2$  and  $b_2 < c_2$ .*

*Proof* The variational matrix at the equilibrium point  $E_1 = (b_1 - a_1(b_1 - c_1))/b_1, (b_1 - a_1(b_1 - c_1))(b_1 - c_1)/(b_1 c_1), 0$  is given by

$$\mathbf{J}(E_1) = \begin{pmatrix} \frac{a_1 (b_1^2 - c_1^2) - b_1^2}{b_1^2} & -\frac{a_1 c_1^2}{b_1^2} & 0 \\ \frac{(b_1 - c_1)^2}{b_1} & -\frac{(b_1 - c_1)c_1}{b_1} & -a_2 \\ 0 & 0 & b_2 - c_2 \end{pmatrix}.$$

The eigenvalues of variational matrix at  $E_1$  are  $b_2 - c_2$  and the roots of the equation

$$\lambda^2 - \left( \frac{a_1 (b_1^2 - c_1^2) - b_1^2}{b_1^2} - \frac{(b_1 - c_1)c_1}{b_1} \right) \lambda + \frac{(b_1 - c_1)c_1}{b_1} - \frac{a_1 c_1 (b_1 - c_1)^2}{b_1^2} = 0.$$

Hence, the equilibrium point  $E_1$  is locally asymptotically stable if  $b_2 < c_2$  and

$$b_1 c_1 (b_1 - c_1) > a_1 (b_1^2 - c_1^2) - b_1^2.$$

□

From biological point of view, the stability of the nontrivial steady state  $E^* = (N^*, P^*, Z^*)$  which ensures the coexistence of the three species is of interest.

**Theorem 3** *The interior equilibrium point  $E^* = (N^*, P^*, Z^*)$  is locally asymptotically stable if  $(a_2 b_2 - b_2 c_1 + a_2 c_2)^2 < b_1 b_2^2 c_1 + a_2 b_1 (b_2 - c_2)^2$ .*

*Proof* The variational matrix at the equilibrium point  $E^* = (N^*, P^*, Z^*)$  is given by

$$\mathbf{J}(E^*) = \begin{pmatrix} J_{11} & J_{12} & J_{13} \\ J_{21} & J_{22} & J_{23} \\ J_{31} & J_{32} & J_{33} \end{pmatrix},$$

where

$$J_{11} = -\frac{b_1^2 b_2^2 (1 - a_1) + a_1 (a_2 (b_2 - c_2) + b_2 c_1)^2}{b_1^2 b_2^2},$$

$$J_{12} = -\frac{a_1 (b_2 c_1 + a_2 (b_2 - c_2))^2}{b_1^2 b_2^2}, \quad J_{13} = 0,$$

$$J_{21} = \frac{(a_2 (b_2 - c_2) - b_2 (b_1 - c_1))^2}{b_1 b_2^2},$$

$$J_{22} = \frac{1}{b_1 b_2^2} \left( -b_1 b_2^2 c_1 - a_2 b_1 (b_2 - c_2)^2 + (a_2 b_2 - b_2 c_1 + a_2 c_2)^2 \right),$$

$$J_{23} = -\frac{a_2 c_2^2}{b_2^2}, \quad J_{31} = 0,$$

$$J_{32} = \frac{(b_2 - c_2)^2}{b_2},$$

$$J_{33} = -\frac{(b_2 - c_2)c_2}{b_2}.$$

The characteristic equation at the interior equilibrium point  $E^*$  is

$$\lambda^3 + Q_1 \lambda^2 + Q_2 \lambda + Q_3 = 0,$$

where

$$Q_1 = -(J_{11} + J_{22} + J_{33}),$$

$$Q_2 = J_{11} J_{22} - J_{12} J_{21} + (J_{11} + J_{22}) J_{33} - J_{23} J_{32},$$

$$Q_3 = J_{11} J_{23} J_{32} - J_{11} J_{22} J_{33} + J_{12} J_{21} J_{33}.$$

It is clear that

$$J_{11} < 0, \quad J_{12} < 0, \quad J_{21} > 0, \quad J_{23} < 0,$$

$$J_{32} > 0, \quad J_{33} < 0.$$

Here  $Q_1 > 0$  and  $Q_2 > 0$  if  $J_{22} < 0$  and obviously  $Q_3 > 0$ .

Now  $Q_1 Q_2 - Q_3 = (J_{22} + J_{33})(J_{23} J_{32} - J_{22} J_{33}) - (J_{11} + J_{22} + J_{33})(J_{11} J_{22} - J_{12} J_{21} + J_{11} J_{33}) - J_{12} J_{21} J_{33}$ . If  $J_{22} < 0$ , then  $(J_{22} + J_{33})(J_{23} J_{32} - J_{22} J_{33}) > 0$ ,  $J_{12} J_{21} J_{33} > 0$ ,  $J_{11} + J_{22} + J_{33} < 0$ , and  $J_{11} J_{22} - J_{12} J_{21} + J_{11} J_{33} > 0$ . Thus,  $Q_1 Q_2 - Q_3 > 0$ .

Therefore, the non-spatial model (2) is locally stable at the interior equilibrium  $E^* = (N^*, P^*, Z^*)$  if  $(a_2 b_2 - b_2 c_1 + a_2 c_2)^2 < b_1 b_2^2 c_1 + a_2 b_1 (b_2 - c_2)^2$ . □

### 2.2 Dynamics of the spatial model (2)

The spatial model (2) is to be analyzed under the following non-zero initial conditions

$$N(x, y, 0) > 0, \quad P(x, y, 0) > 0, \quad Z(x, y, 0) > 0, \\ (x, y) \in \Omega = [0, Lx] \times [0, Ly] \tag{3}$$

and zero-flux boundary conditions

$$\frac{\partial N}{\partial \mathbf{n}} = \frac{\partial P}{\partial \mathbf{n}} = \frac{\partial Z}{\partial \mathbf{n}} = 0, \quad (x, y) \in \partial\Omega. \tag{4}$$

In the above,  $Lx$  and  $Ly$  give the size of the model in the directions of  $x$  and  $y$ , respectively.  $\mathbf{n}$  is the outward unit normal vector of the boundary  $\partial\Omega$ , which we assume is smooth. The main reason for choosing such boundary conditions is that we are interested in the self-organization of pattern; zero-flux conditions imply no external input [23].

Next, we will analyze the stability of the positive equilibrium  $E^*$  of the reaction–diffusion model (2).

**Theorem 4** *If  $P + Z > a_1 a_2 P^* Z^* / (b_1 N^* (P^* + Z^*))$  and  $a_1 / b_1 > P^* / Z^* > b_2 / a_2$ , then the uniform steady state  $E^* = (N^*, P^*, Z^*)$  of model (2) is globally asymptotically stable.*

*Proof* Define a Liapunov function

$$V_1(N, P, Z) = \int_{N^*}^N \frac{\chi - N^*}{\chi} d\chi + \int_{P^*}^P \frac{\xi - P^*}{\xi} d\xi \\ + \int_{Z^*}^Z \frac{\eta - Z^*}{\eta} d\eta. \tag{5}$$

Note that  $V_1(N, P, Z)$  is nonnegative and  $V_1(N, P, Z) = 0$  if and only if  $(N(t), P(t), Z(t)) = (N^*, P^*, Z^*)$ . Furthermore, the time derivative of  $V_1$  along the solutions of model (2) without diffusion is

$$\frac{dV_1}{dt} = \frac{N - N^*}{N} \frac{dN}{dt} + \frac{P - P^*}{P} \frac{dP}{dt} + \frac{Z - Z^*}{Z} \frac{dZ}{dt}.$$

Substituting the expressions of  $dN/dt$ ,  $dP/dt$ , and  $dZ/dt$  from model (2) in the absence of diffusion, we obtain

$$\frac{dV_1}{dt} = (N - N^*) \left( 1 - N - \frac{a_1 P}{N + P} \right) \\ + (P - P^*) \left( \frac{b_1 N}{N + P} - c_1 - \frac{a_2 Z}{P + Z} \right) \\ + (Z - Z^*) \left( \frac{b_2 P}{P + Z} - c_2 \right).$$

Using the fact that

$$N^* + \frac{a_1 P^*}{N^* + P^*} = 1, \quad \frac{b_1 N^*}{N^* + P^*} - \frac{a_2 Z^*}{P^* + Z^*} = c_1, \\ \frac{b_2 P^*}{P^* + Z^*} = c_2,$$

and if  $b_1 N^* (P^* + Z^*) (P + Z) > a_1 a_2 P^* Z^*$ ,  $\frac{a_1}{b_1} > \frac{P^*}{Z^*} > \frac{b_2}{a_2}$ , we can get

$$\frac{dV_1}{dt} \leq - \left( 1 - \frac{a_1 P^*}{(N^* + P^*)(N + P)} \right) (N - N^*)^2 \\ - \left( \frac{b_1 N^*}{(N + P)(N^* + P^*)} - \frac{a_2 Z^*}{(P^* + Z^*)(P + Z)} \right) \\ \times (P - P^*)^2 \\ - \frac{b_2 P^*}{(P + Z)(P^* + Z^*)} (Z - Z^*)^2 \\ \leq 0.$$

Then, we choose the following Liapunov function for the spatial model (2)

$$V_2 = \iint_{\Omega} V_1(N, P, Z) d\Lambda, \tag{6}$$

and differentiating  $V_2$  with respect to time  $t$  along the solutions of model (2), we have

$$\frac{dV_2}{dt} = \iint_{\Omega} \frac{dV_1}{dt} d\Lambda + \iint_{\Omega} \left( d_1 \frac{\partial V_1}{\partial N} \Delta N + d_2 \frac{\partial V_1}{\partial P} \Delta P \\ + d_3 \frac{\partial V_1}{\partial Z} \Delta Z \right) d\Lambda.$$

Using Green’s first identity in the plane

$$\iint_{\Omega} F \nabla^2 G dx dy = \int_{\partial\Omega} F \frac{\partial G}{\partial \mathbf{n}} ds - \iint_{\Omega} (\nabla F \cdot \nabla G) dx dy. \tag{7}$$

And considering the zero-flux boundary conditions (4), we obtain

$$\frac{dV_2}{dt} = \iint_{\Omega} \frac{dV_1}{dt} d\Lambda \\ - d_1 \iint_{\Omega} \frac{\partial^2 V_1}{\partial N^2} \left( \left( \frac{\partial N}{\partial x} \right)^2 + \left( \frac{\partial N}{\partial y} \right)^2 \right) d\Lambda \\ - d_2 \iint_{\Omega} \frac{\partial^2 V_1}{\partial P^2} \left( \left( \frac{\partial P}{\partial x} \right)^2 + \left( \frac{\partial P}{\partial y} \right)^2 \right) d\Lambda \\ - d_3 \iint_{\Omega} \frac{\partial^2 V_1}{\partial Z^2} \left( \left( \frac{\partial Z}{\partial x} \right)^2 + \left( \frac{\partial Z}{\partial y} \right)^2 \right) d\Lambda,$$

where

$$\frac{\partial^2 V_1}{\partial N^2} > 0, \quad \frac{\partial^2 V_1}{\partial P^2} > 0, \quad \frac{\partial^2 V_1}{\partial Z^2} > 0.$$

From the above analysis, if  $dV_1/dt < 0$ , then we have  $dV_2/dt < 0$ . This implies that if the positive equilibrium point  $E^* = (N^*, P^*, Z^*)$  of model (2) without diffusion is globally asymptotically stable, then in the presence of diffusion,  $E^* = (N^*, P^*, Z^*)$  of model (2) will remain globally asymptotically stable.  $\square$

To better understand the spatial dynamics of model (2), we consider the linearized form of (2) about  $E^* = (N^*, P^*, Z^*)$  as follows:

$$\begin{aligned} \frac{\partial U_1}{\partial t} &= J_{11}U_1 + J_{12}U_2 + J_{13}U_3 + d_1 \nabla^2 U_1, \\ \frac{\partial U_2}{\partial t} &= J_{21}U_1 + J_{22}U_2 + J_{23}U_3 + d_2 \nabla^2 U_2, \\ \frac{\partial U_3}{\partial t} &= J_{31}U_1 + J_{32}U_2 + J_{33}U_3 + d_3 \nabla^2 U_3, \end{aligned} \tag{8}$$

where we will introduce small perturbations  $U_1 = N - N^*$ ,  $U_2 = P - P^*$ , and  $U_3 = Z - Z^*$ , ( $|U_1|, |U_2|$  and  $|U_3| \ll 1$ ). Define  $\mathbf{D} = \text{diag}(d_1, d_2, d_3)$  as the diffusion matrix. Referring to Malchow et al. [20], any solutions of model (8) can be expanded into a Fourier series

$$\begin{aligned} U_1(\mathbf{r}, t) &= \sum_{i,j=0}^{\infty} n_{ij}(\mathbf{r}, t) = \sum_{i,j=0}^{\infty} \alpha_{ij}(t) \sin \mathbf{kr}, \\ U_2(\mathbf{r}, t) &= \sum_{i,j=0}^{\infty} p_{ij}(\mathbf{r}, t) = \sum_{i,j=0}^{\infty} \beta_{ij}(t) \sin \mathbf{kr}, \\ U_3(\mathbf{r}, t) &= \sum_{i,j=0}^{\infty} z_{ij}(\mathbf{r}, t) = \sum_{i,j=0}^{\infty} \gamma_{ij}(t) \sin \mathbf{kr}, \end{aligned} \tag{9}$$

where  $\mathbf{r} = (x, y)$  and  $0 < x < Lx$ ,  $0 < y < Ly$ . Note that  $\mathbf{k} = (k_i, k_j)$  and  $k_i = i\pi/Lx$ ,  $k_j = j\pi/Ly$  are the corresponding wavenumbers.

Having substituted  $n_{ij}$ ,  $p_{ij}$ , and  $z_{ij}$  with (8), we obtain

$$\begin{aligned} \frac{d\alpha_{ij}}{dt} &= (J_{11} - d_1 k^2)\alpha_{ij} + J_{12}\beta_{ij} + J_{13}\gamma_{ij}, \\ \frac{d\beta_{ij}}{dt} &= J_{21}\alpha_{ij} + (J_{22} - d_2 k^2)\beta_{ij} + J_{23}\gamma_{ij}, \\ \frac{d\gamma_{ij}}{dt} &= J_{31}\alpha_{ij} + J_{32}\beta_{ij} + (J_{33} - d_3 k^2)\gamma_{ij}, \end{aligned} \tag{10}$$

where  $k^2 = k_i^2 + k_j^2$ . A general solution of (10) has the form  $C_1 e^{\lambda_1 t} + C_2 e^{\lambda_2 t} + C_3 e^{\lambda_3 t}$ , the constants  $C_1$ ,  $C_2$ , and  $C_3$  are determined by the initial conditions (3) and

the exponents  $\lambda_1$ ,  $\lambda_2$ , and  $\lambda_3$  are the eigenvalues of the following matrix:

$$\hat{\mathbf{J}} = \begin{pmatrix} J_{11} - d_1 k^2 & J_{12} & J_{13} \\ J_{21} & J_{22} - d_2 k^2 & J_{23} \\ J_{31} & J_{32} & J_{33} - d_3 k^2 \end{pmatrix}. \tag{11}$$

Correspondingly,  $\lambda_1$ ,  $\lambda_2$ , and  $\lambda_3$  arise as the solution of the following equation:

$$\lambda^3 + A(k^2)\lambda^2 + B(k^2)\lambda + C(k^2) = 0, \tag{12}$$

where

$$\begin{aligned} A(k^2) &= (d_1 + d_2 + d_3)k^2 - (J_{11} + J_{22} + J_{33}), \\ B(k^2) &= (d_1 d_2 + d_1 d_3 + d_2 d_3)k^4 - (d_1(J_{22} + J_{33}) \\ &\quad + d_2(J_{11} + J_{33}) + d_3(J_{11} + J_{22}))k^2 \\ &\quad + (J_{11}J_{22} + J_{11}J_{33} + J_{22}J_{33} - J_{12}J_{21} - J_{23}J_{32}), \\ C(k^2) &= d_1 d_2 d_3 k^6 - (d_1 d_2 J_{33} + d_1 d_3 J_{22} + d_2 d_3 J_{11})k^4 \\ &\quad + (d_1 J_{22} J_{33} - d_1 J_{23} J_{32} + d_2 J_{11} J_{33} - d_2 J_{13} J_{31} \\ &\quad + d_3 J_{11} J_{22} - d_3 J_{12} J_{21})k^2 \\ &\quad + (J_{11} J_{23} J_{32} + J_{12} J_{21} J_{33} - J_{11} J_{22} J_{33}). \end{aligned}$$

It is well known that the reaction–diffusion model leads to the characterization of two basic types of symmetry breaking bifurcations—Hopf and Turing bifurcations, which are responsible for the emergence of spatiotemporal patterns. Where the space-independent Hopf bifurcation breaks the temporal symmetry of a system and gives rise to oscillations that are uniform in space and periodic in time. The Turing bifurcation breaks spatial symmetry, leading to the formation of patterns that are stationary in time and oscillatory in space [1,40,43].

By using the bifurcation theory, the Hopf bifurcation, mathematically speaking, occurs when

$$\text{Im}(\lambda(k)) \neq 0, \quad \text{Re}(\lambda(k)) = 0 \quad \text{at } k = 0.$$

And the Turing bifurcation occurs when

$$\text{Im}(\lambda(k)) = 0, \quad \text{Re}(\lambda(k)) = 0 \quad \text{at } k \neq 0.$$

Setting parameters  $a_2 = 0.52$ ,  $b_1 = 1.5$ ,  $b_2 = 2$ ,  $c_2 = 1.05$ ,  $d_1 = 0.02$ ,  $d_2 = 0.2$ , and  $d_3 = 1$ , linear stability analysis yields a bifurcation diagram for varying  $a_1$  and  $c_1$  as shown in Fig. 1. In the figure, the red solid line is Hopf bifurcation curve,

the blue-dotted line is Turing bifurcation curve. And the black-dashed line is critical state that above the dashed line, prey and their predators cannot coexist; under the line, the three species are coexistence. The Hopf and Turing bifurcation curves separate the coexistence space into four domains. Domain I is the region of pure Turing instability. When the parameters correspond to domain II, which is located above all two bifurcation lines, both Hopf and Turing instability occur. Domain III is the region of pure Hopf instability. Domain IV, located below two bifurcation curves, the uniform steady state is the only stable solution of model (2).

### 3 Pattern formation

In this section, we perform extensive numerical simulations of the spatially extended model (2) in two-dimensional space to illustrate the results obtained in Sect. 2, and the qualitative results are shown here. We run the simulations until they reach a stationary state or until they show a behavior that does not seem to change its characteristics anymore. Since the three species exhibit qualitatively similar behavior, for illustration, only the prey abundance is shown in this paper. All our numerical simulations employ non-zero initial conditions (3) and zero-flux boundary conditions (4) with a system size of  $Lx \times Ly$ , where  $Lx = Ly = 200$  discretized through  $x \rightarrow (x_0, x_1, x_2, \dots, x_n)$  and  $y \rightarrow (y_0, y_1, y_2, \dots, y_n)$  with  $n = 600$ . We use the standard five-point approximation for the two-dimensional Laplacian which in the discrete model describes diffusion [9]. The time evolution can be solved by using an explicit Euler method, which means approximating the value of the concentration at the next time step based on the rate of change of the concentration in the previous time step. More precisely, the concentrations  $(N_{i,j}^{n+1}, P_{i,j}^{n+1}, Z_{i,j}^{n+1})$  at the moment  $(n + 1)\tau$  at the mesh point  $(x_i, y_j)$  are given by

$$\begin{aligned} N_{i,j}^{n+1} &= N_{i,j}^n + \tau d_1 \Delta_h N_{i,j}^n + \tau f_1(N_{i,j}^n, P_{i,j}^n, Z_{i,j}^n), \\ P_{i,j}^{n+1} &= P_{i,j}^n + \tau d_2 \Delta_h P_{i,j}^n + \tau f_2(N_{i,j}^n, P_{i,j}^n, Z_{i,j}^n), \\ Z_{i,j}^{n+1} &= Z_{i,j}^n + \tau d_3 \Delta_h Z_{i,j}^n + \tau f_3(N_{i,j}^n, P_{i,j}^n, Z_{i,j}^n), \end{aligned}$$

with the Laplacian defined by

$$\Delta_h N_{i,j}^n = \frac{N_{i+1,j}^n + N_{i-1,j}^n + N_{i,j+1}^n + N_{i,j-1}^n - 4N_{i,j}^n}{h^2},$$

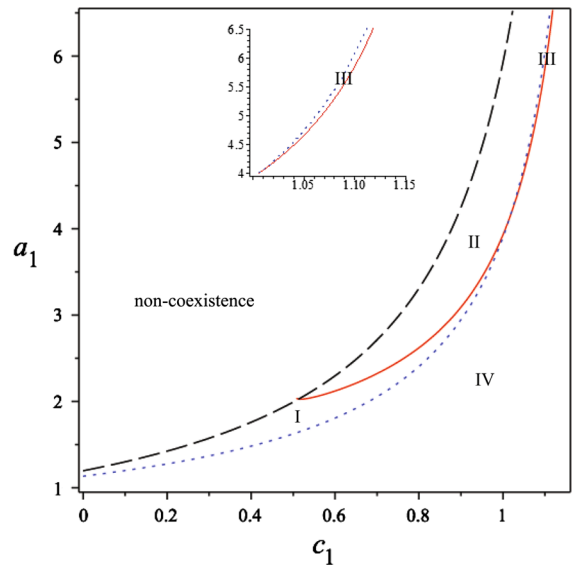


**Fig. 1** Bifurcation diagram for model (2) using  $c_1$  and  $a_1$  as parameters with  $a_2 = 0.52$ ,  $b_1 = 1.5$ ,  $b_2 = 2$ ,  $c_2 = 1.05$ ,  $d_1 = 0.02$ ,  $d_2 = 0.2$ , and  $d_3 = 1$ . The red solid line is Hopf bifurcation curve, the blue-dotted line is Turing bifurcation curve, and the black-dashed line is the dividing curve of coexistence and non-coexistence of prey and their predators. Hopf and Turing bifurcation curves separate the coexistence parameter space into four domains. (Color figure online)

where the space step size  $h = 1/4$  and a time step size of  $\tau = 1/100$ .

We are mainly interested in investigating the behavior of model (2) around the interior equilibrium point, so we shall put emphasis on the positive equilibrium point  $E^* = (N^*, P^*, Z^*)$ . The entire system is initially placed in the stationary state  $(N^*, P^*, Z^*)$  and the propagation velocity of the initial perturbation is thus of the order of  $5 \times 10^{-4}$  space units per time unit [28]. Based on the analysis of Sect. 2 and bifurcation diagram (see Fig. 1), the results of computer simulations show that the type of the model dynamics is determined by the values of  $a_1$  and  $c_1$ . For different sets of parameters, the features of the spatial patterns become essentially different if  $a_1$  exceeds the Turing and Hopf bifurcation curves, respectively, which depend on  $c_1$ .

In the following Figs. 2, 3, and 4, which we consider the pattern formation for the parameters  $(c_1, a_1)$  located in domain I (see Fig. 1), the region of pure Turing instability occurs while Hopf stability occurs, four different snapshots during the temporal evolution of model (2) are presented in two-dimensional space. These figures are the prey species density levels as a

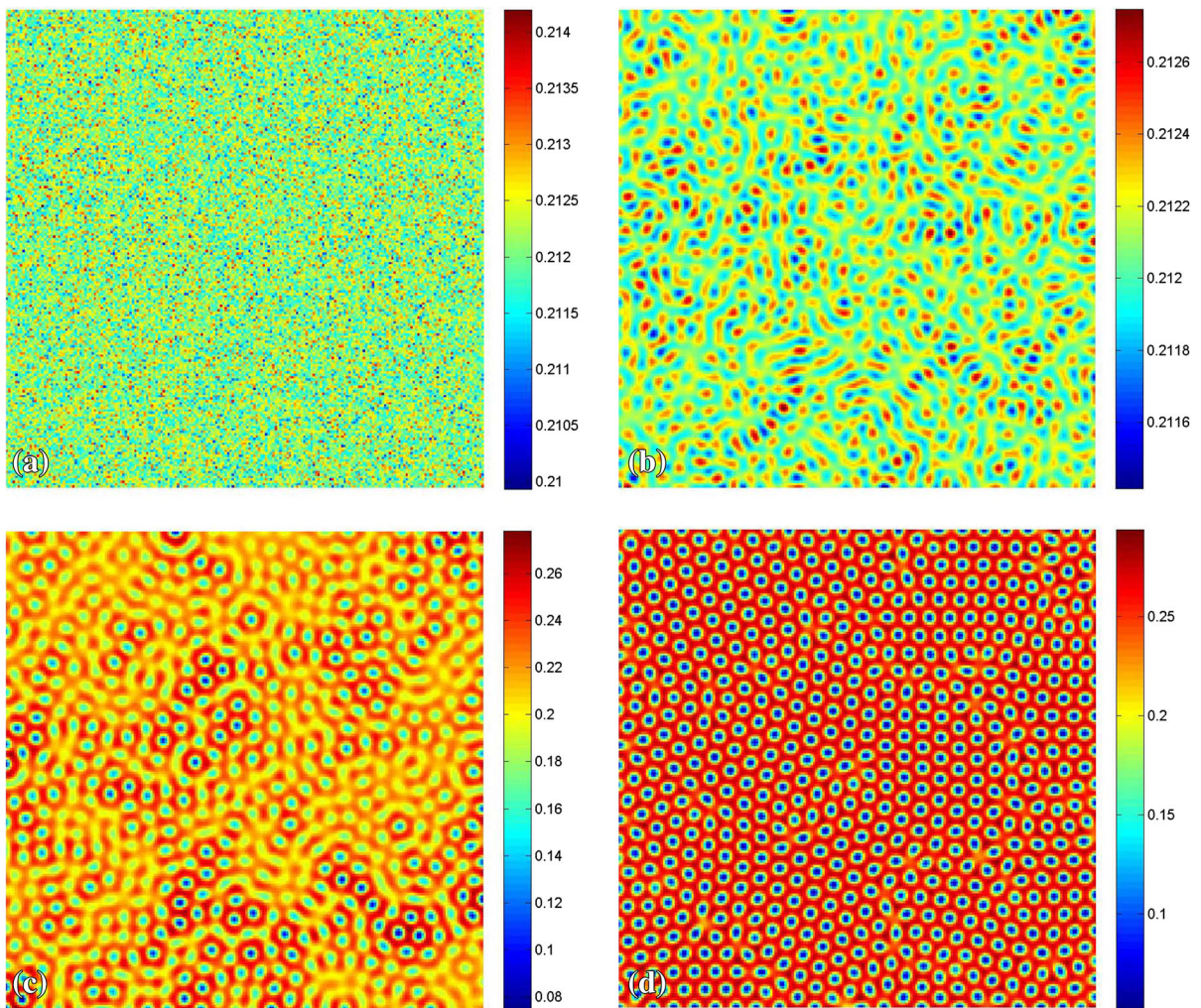


**Fig. 2** Snapshots of contour pictures of the time evolution of prey  $N$  at different times with  $a_1 = 1.838$  and other parameters are taken as (13) in the text. Time steps: **a**  $t = 0$ , **b**  $t = 100$ , **c**  $t = 1,000$ , and **d**  $t = 5,000$

function of space and time on a color scale, with blue corresponding to the lowest density state and red corresponding to the highest density state. Figures 2, 3, and 4 depict spatial patterns in two-dimensional space under different values of  $a_1$ , respectively, and other parameters are fixed as

$$\begin{aligned} a_2 = 0.52, \quad b_1 = 1.5, \quad b_2 = 2, \quad c_1 = 0.61, \\ c_2 = 1.05, \quad d_1 = 0.02, \quad d_2 = 0.2, \quad d_3 = 1. \end{aligned} \quad (13)$$

With the parameters set, the critical value of Turing bifurcation is  $a_{1T} = 1.82864$  and that of Hopf bifurcation is  $a_{1H} = 2.13736$ . So, the value of  $a_1$  we adopt is between  $a_{1T}$  and  $a_{1H}$ .

In Fig. 2, we plot the evolution of spatial pattern for prey  $N$  of the spatial model (2) at time  $t = 0, 100, 1,000$ , and  $5,000$ . Here, we choose  $a_1 = 1.838$  and the nontrivial stationary state is  $(N^*, P^*, Z^*) = (0.21211, 0.15914, 0.14399)$ . In this case, one can see that after irregular transient patterns (see Fig. 2a–c), the pattern takes a long time to settle down and the regular spotted patterns prevail over the whole domain at last (see Fig. 2d), which is time-independent. This pattern consists of blue spots (minimum density of  $N$ ) on a red (maximum density of  $N$ ) background, that is, isolated zones with low population densities. For this type pattern, we called “cold” spots pattern. Baumann et al. [1] used the names “hot spots”



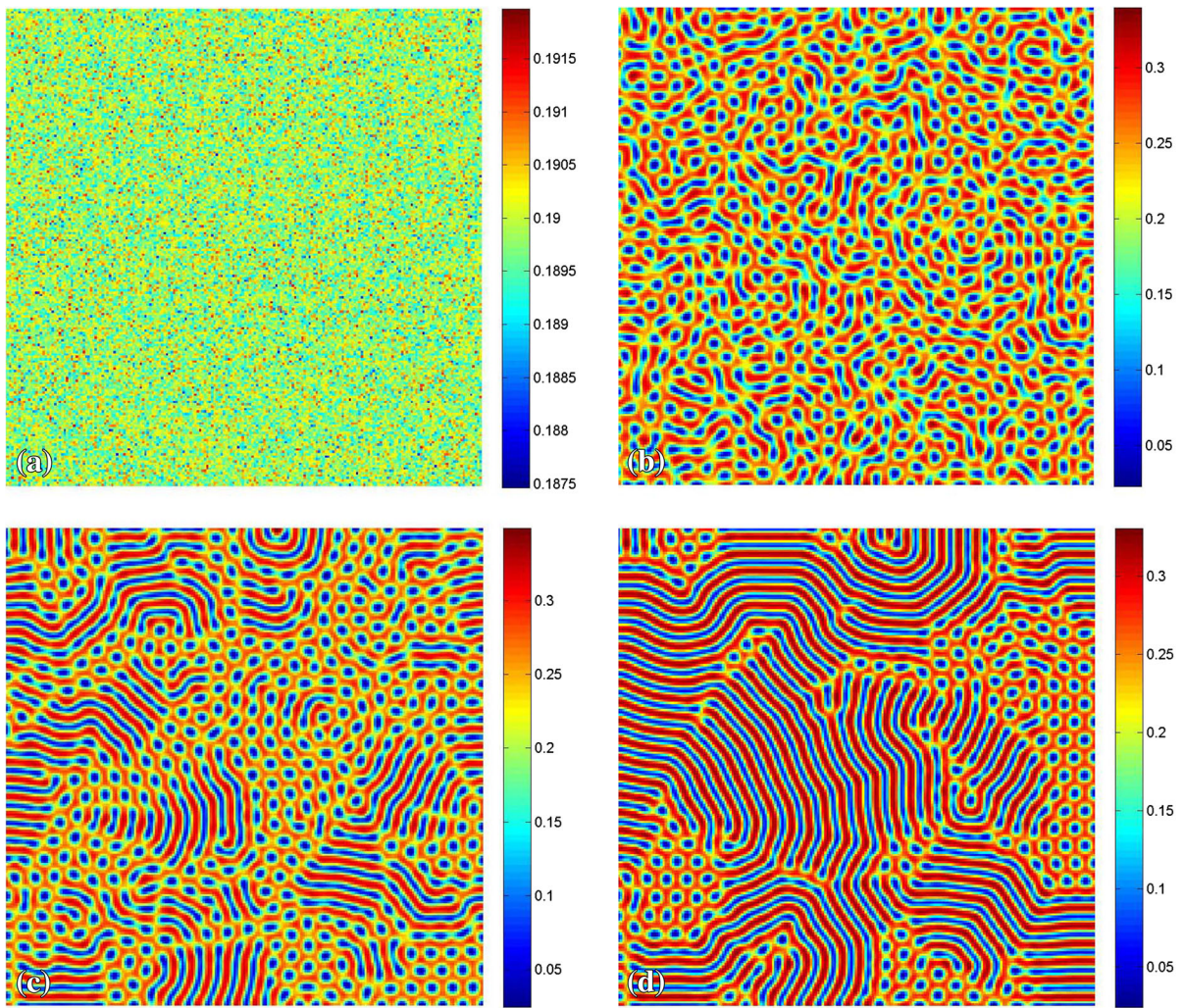


**Fig. 3** Snapshots of contour pictures of the time evolution of prey  $N$  at different times with  $a_1 = 1.89$  and other parameters are taken as (13). Time steps: **a**  $t = 0$ , **b**  $t = 200$ , **c**  $t = 1,000$ , and **d**  $t = 5,000$

and “cold spots” in pattern formation of predator–prey model. von Hardenberg et al. [36] in describing the vegetation pattern used the words “spots” and “holes,” corresponding to “hot spots” and “cold spots,” respectively.

When increasing  $a_1$  to  $a_1 = 1.89$  and other parameters values are fixed as (13), Fig. 3 shows the evolution of spatial pattern of  $N$  at  $t = 0, 200, 1,000$ , and  $5,000$  of model (2). In this case, starting with the steady state  $(N^*, P^*, Z^*) = (0.18982, 0.14242, 0.12886)$ , the random initial distribution leads to the formation of stripe–spots mixtures (see Fig. 3d).

As the parameter  $a_1$  is further increased, there is a drastic influence on the pattern formation, which is

illustrated in Fig. 4 with  $a_1 = 2.03$  and other parameters are taken as (13). Figure 4 shows the evolution of spatial pattern of  $N$  at  $t = 0, 200, 1,000$ , and  $5,000$ . Starting with  $(N^*, P^*, Z^*) = (0.12981, 0.09739, 0.08812)$ , the random perturbations lead to the formation of stripes and spots (see Fig. 4b, c), and ending with stripes only (see Fig. 4d).

For the sake of learning more about these evolutionary processes, in Fig. 5, we illustrate time-series plots for prey  $N$ , intermediate predator  $P$ , and top predator  $Z$  of the spatial model (2) with initial value  $(N^*, P^*, Z^*)$  and different  $a_1$ , respectively, corresponding to the patterns in Figs. 2, 3, and 4. In Fig. 5a,  $a_1 = 1.838$ , corresponding to Fig. 2, one can see that

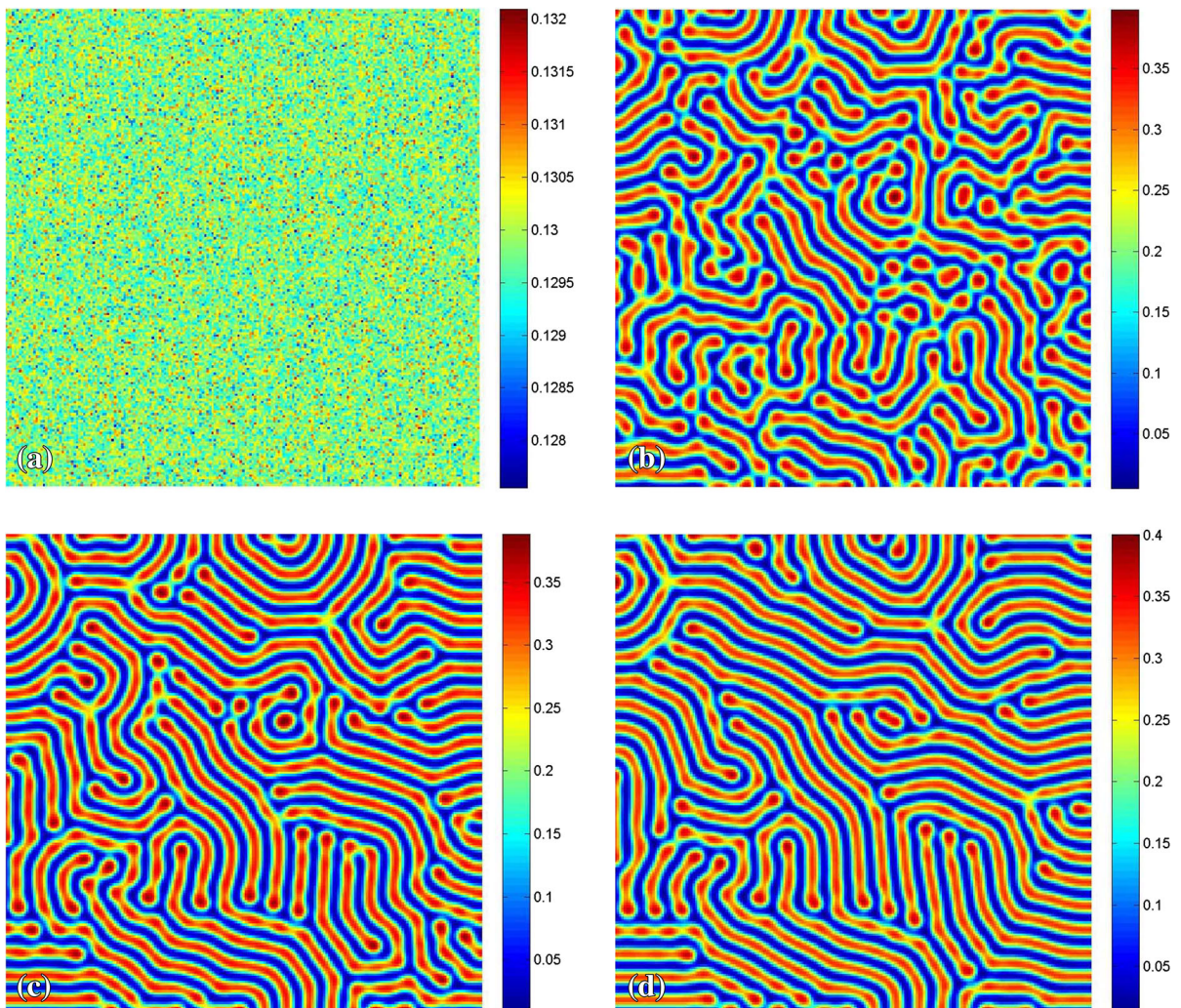


**Fig. 4** Snapshots of contour pictures of the time evolution of prey  $N$  at different times with  $a_1 = 2.03$  and other parameters are taken as (13). Time steps: **a**  $t = 0$ , **b**  $t = 200$ , **c**  $t = 1,000$ , and **d**  $t = 5,000$

when  $t > 2,000$  the three-species population change slowly, and  $N \in (0.22, 0.23)$ ,  $P \in (0.162, 0.164)$ , and  $Z \in (0.1429, 0.1431)$ . In Fig. 5b,  $a_1 = 1.89$ , corresponding to Fig. 3, the prey  $N$  and intermediate predator  $P$  population change over time, and when  $t > 1,000$ ,  $Z \in (0.127, 0.13)$ . In Fig. 5c,  $a_1 = 2.03$ , corresponding to Fig. 4, the prey  $N$  and intermediate predator  $P$  population change over time, and when  $t > 1,000$ ,  $Z \in (0.103, 0.108)$ . That is to say, when  $a_1$  increases from 1.838 to 2.03, namely, the ingestion rate of intermediate predator  $P$  increases, the values of prey  $N$  change with time and that of top predator  $Z$  will decrease.

In the following, we consider the pattern formation in domain II (see Fig. 1), in which both Turing and Hopf instability occur. When other parameters are fixed as (13), we choose  $a_1$  between the Hopf bifurcation curve  $a_{1H} = 2.13736$  and the maximize value of the coexistence of prey and their predators  $a_{1c} = 2.33281$ .

In Fig. 6, we show two typical patterns obtained with model (2) at time  $t = 5,000$  and time-series plots for three species. The patterns consist of red stripe-spots and spots on a blue background, respectively. We call them as “hot stripe-spots” (see Fig. 6a) and “hot spots” (see Fig. 6b). In Fig. 6a, with  $a_1 = 2.139$  and other parameters are taken as (13),  $(N^*, P^*, Z^*) =$

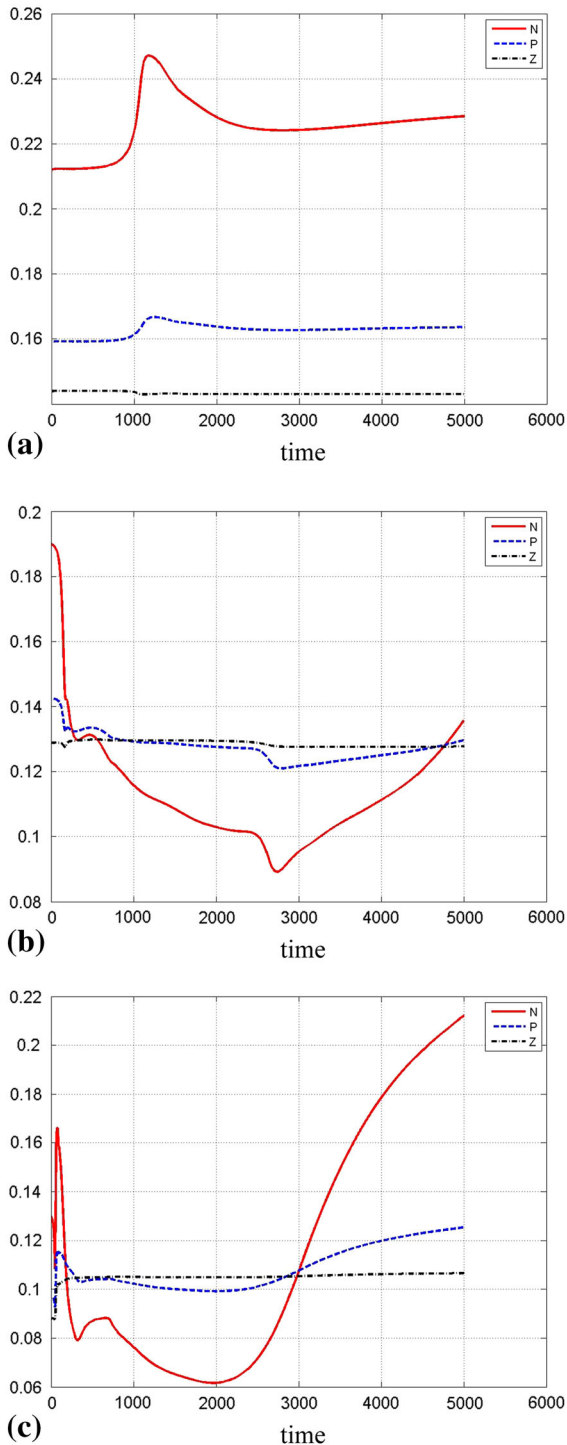


**Fig. 5** Time-series plots of three species of model (2). **a**  $a_1 = 1.838$ , **b**  $a_1 = 1.89$ , **c**  $a_1 = 2.03$ , and other parameters are taken as (13)

(0.08308, 0.06234, 0.05640), the hot stripe–spots are isolated zones with high prey densities. In this case, the predators are in low density obviously. While in Fig. 6b, increasing  $a_1$  to  $a_1 = 2.3$  and other parameters are fixed as (13),  $(N^*, P^*, Z^*) = (0.01407, 0.01055, 0.00955)$ , hot spots are isolated zones with high prey density. From Fig. 6a, b, one can see that a transition from stripe–spots mixture patterns growth to spots replication, that is, stripes decay and the spots pattern emerges. In Fig. 6c, time-series plots with  $a_1 = 2.139$ , corresponding to Fig. 6a, when  $t > 1,000$ ,  $N \in (0.22, 0.27)$ ,  $P \in (0.11, 0.12)$ , and  $Z \in (0.09, 0.093)$ . That shows the stable population distribution of the three species. In Fig. 6d,  $a_1 = 2.3$ , corresponding to Fig. 6b, when  $t < 1,000$ , the three-species population give rise to drastically oscillations, while  $t > 1,000$  the values of prey  $N$ , intermediate predator  $P$ , and top predator  $Z$  are asymptotically stable. It is proved that the parameter  $a_1$  has a stabilizing effect, that is, increases the local stability of the interior equilibrium  $E^* = (N^*, P^*, Z^*)$ .

Moreover, in order to investigate quantitatively the evolution of spatial patterns of model (2) with parameter  $a_1$  in domain II (see Fig. 1), in Fig. 7 we show spacetime plots which display the evolution process of prey  $N$  throughout time  $t$  and space  $x$  with different  $a_1$ .

The method of spacetime plots is to let  $y$  be a constant, choose the line  $y = 100$  from each pattern snapshot, and pile these lines in time order [31]. In Fig. 7, time increases from bottom to top, and the horizontal axis represents the spatial location. From Fig. 7a, b, the single parameter of model (2) namely  $a_1$ , which is the ingestion rate of  $P$ , can lead to dramatic changes in the qualitative dynamics of solutions. From a biological perspective, the ingestion rate plays an important role in the pattern formation of the prey, that is, changes the pattern into irregular spatial pattern with time.

Comparing with Figs. 2, 3, 4, and 6, we can find that these patterns are quite different on account of the varying of  $a_1$  of the spatial model (2). That is, the behavior of the reaction–diffusion model undergoes drastic changes when the varying of parameter  $a_1$ . From these figures, one can see that, with fixed parameters (13), on increasing the control parameter  $a_1$ , a pattern sequence “cold spots  $\rightarrow$  stripe–spots mixtures  $\rightarrow$  stripes  $\rightarrow$  hot stripe–spots mixtures  $\rightarrow$  hot spots” can be observed.

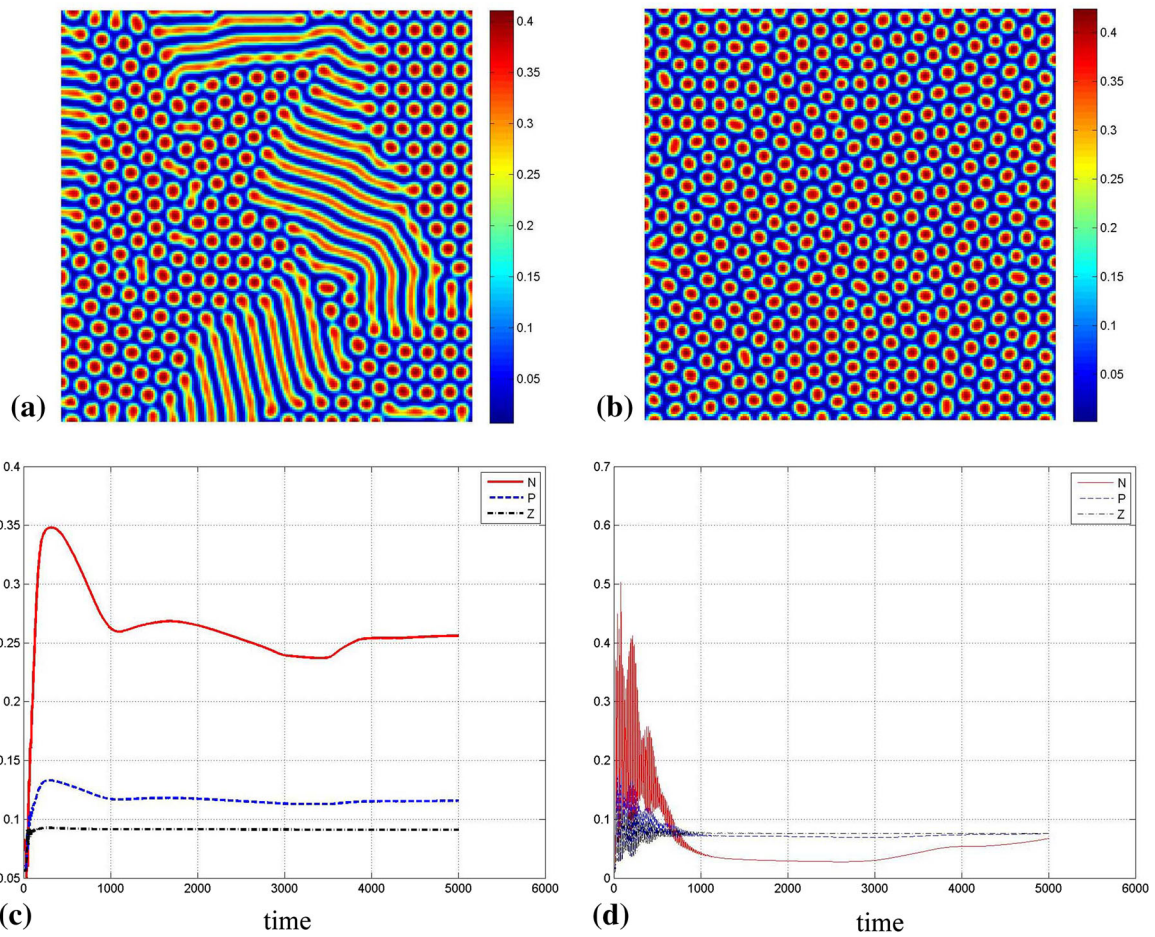


**Fig. 6** Dynamics behavior of varying  $a_1$ . The first column:  $a_1 = 2.139$ , the second column:  $a_1 = 2.3$ , and other parameters are taken as (13). **a, b** Two categories of pattern formations of prey  $N$  at  $t = 5,000$ ; **c, d** time-series plots of three species of model (2)

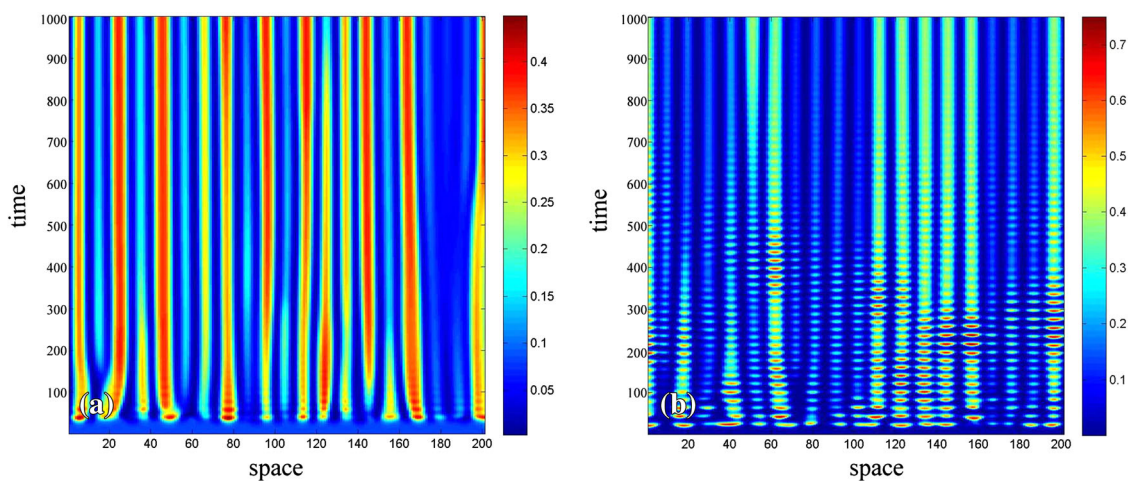


**Fig. 7** Spacetime plots of prey  $N$  of model (2). The time interval shown is 1,000. **a**  $a_1 = 2.139$ , **b**  $a_1 = 2.3$ , and other parameters are taken as (13)

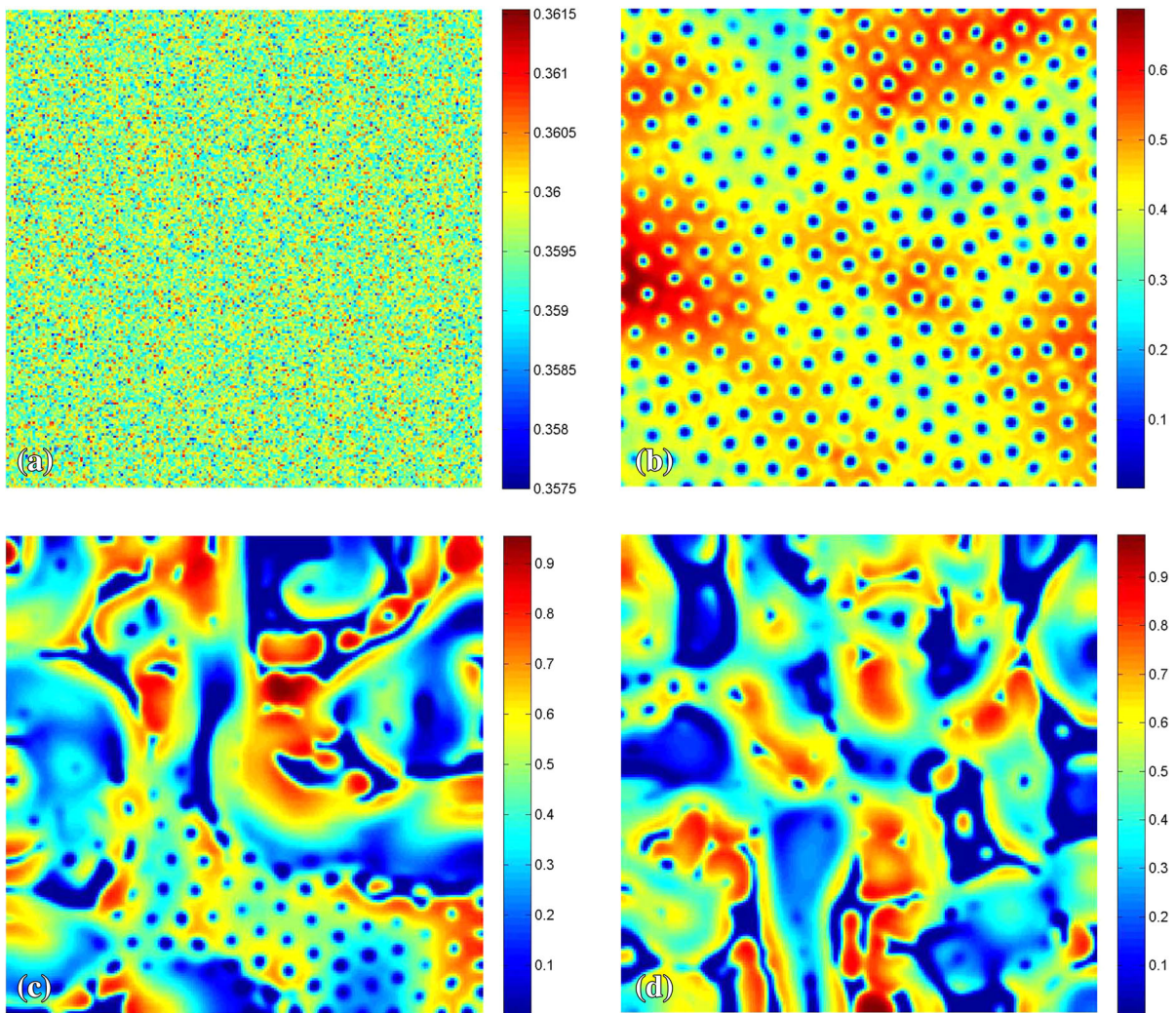


**Fig. 8** Snapshots of contour pictures of the time evolution of prey  $N$  at different times with  $a_1 = 5.11$ ,  $c_1 = 1.065$ , and other parameters are taken as (13). Time steps: **a**  $t = 0$ , **b**  $t = 400$ , **c**  $t = 600$ , and **d**  $t = 5,000$

In addition, when parameters  $(c_1, a_1)$  locate in domain III in Fig. 1, that pure Hopf instability occurs, we consider the pattern formation in Fig. 8. As an example, Fig. 8 shows the evolution of the chaotic pattern of prey  $N$  at  $t = 0, 400, 600$ , and  $5,000$  with  $(c_1, a_1) = (1.065, 5.011)$ . With other fixed parameters (13), the critical value of Hopf bifurcation is  $a_{1H} = 4.95168$  and the Turing bifurcation value equals  $a_{1T} = 5.04843$ . For the sake of learning the pattern formation of Fig. 8 in model (2) further, we show time-series plot of  $N$  and phase portrait in Fig. 9 with parameters used in Fig. 8. In Fig. 9a, one can see that the prey density takes place drastically ruleless fluctua-

tion in time. Figure 9b displays that there exhibits a “local” phase plane of the model obtained in a fixed point  $(N^*, P^*, Z^*) = (0.35955, 0.05152, 0.04661)$  inside the region invaded by the irregular spatiotemporal oscillations.

Figure 10 shows the spacetime plot with  $t$  from 500 to 1,000, which displays the processes of pattern formation of prey  $N$  throughout time  $t$  and space  $x$ , and other parameter values are mentioned in Fig. 8. From that we can see the evolution of wave pattern formation distinctly. That is, the densities of prey  $N$  are oscillating in time with periodic amplitude.

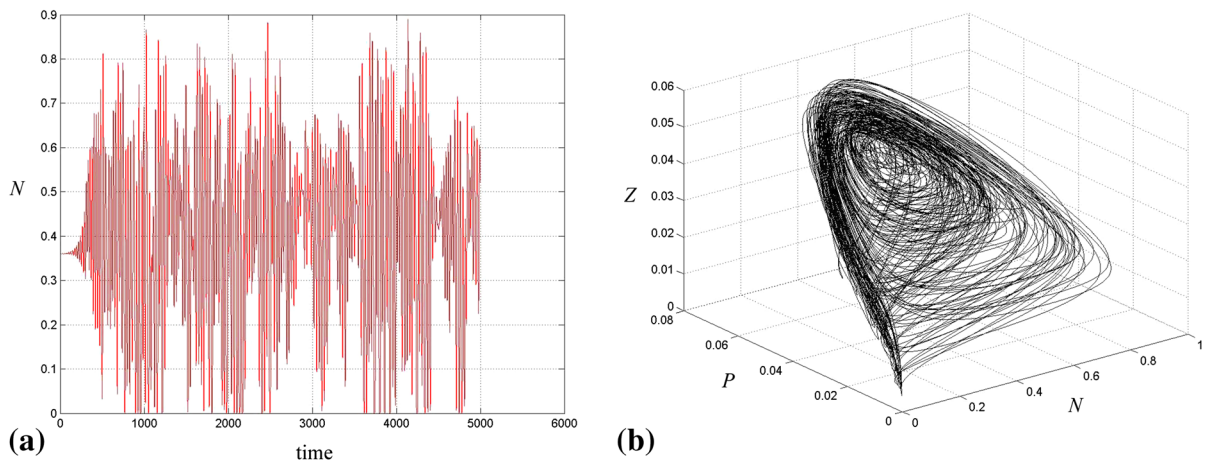


**Fig. 9** Dynamical behavior of model (2). **a** Time-series plot of  $N$  and **b** phase portrait. The parameters are the same as in Fig. 8

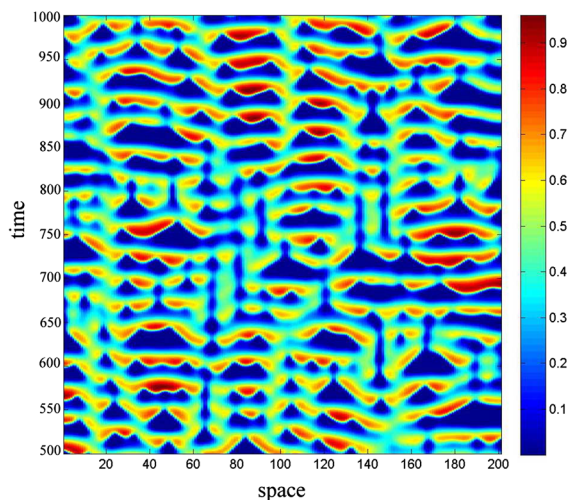


**Fig. 10** Spacetime plot of prey  $N$ . The parameters are the same as in Fig. 8

A plausible biological implication of our findings in this section (see Figs. 2, 3, 4, 5, 6) is that given a prey ( $N$ )–intermediate predator ( $P$ )–top predator ( $Z$ ) interaction, the three species are very sensitive to their effectiveness in catching their preys, which is measured by parameter  $a_1$ . If intermediate predator  $P$  is a voracious one (characterized as having high values of  $a_1$ ) for prey  $N$ , then high (may over prey on  $N$ ) effective intermediate predators  $P$  and low effective top predators  $Z$  may occur. In other words, a more voracious intermediate predator may slightly increase further the average intermediate predator level and decrease average top predator level at the expense of destabilizing such sta-

ble coexistence. If predator  $P$  is not so voracious for prey  $N$ , then high effective top predators  $Z$  occur while low and medium effective ones may endure. Moreover, chaotic phenomena are observed and are controlled by parameters  $a_1$  and  $c_1$  (see Fig. 8). Our results show that, if the parameters are properly chosen, both the general stationary pattern and more interesting pattern can arise as a result of  $a_1$  or  $c_1$ .

#### 4 Conclusions and remarks

In this paper, we make an attempt to investigate the spatiotemporal dynamics in a ratio-dependent spatially extended food chain model analytically and numerically. We adopt the Laplacian operator  $\Delta = \partial^2/\partial x^2 + \partial^2/\partial y^2$  to approximate the diffusive process, i.e., the diffusion of prey species  $N$  and their predators species  $P, Z$  is random in the  $xy$ -plane. By qualitative analysis of the spatial model (2), we observe that the positive equilibrium  $E^* = (N^*, P^*, Z^*)$  of the reaction–diffusion model is globally asymptotically stable if it is globally stable in the absence of diffusion.

Based on the stability and bifurcation analysis, complete variety of stationary and non-stationary patterns are presented for choices of parameter values within the Turing, Turing–Hopf, and Hopf domains. We show the evolution process of pattern formation of the two-dimensional reaction–diffusion model of three-species interaction via numerical simulations. In the numerical simulations, we adopt  $a_1$  and  $c_1$  in model (2) as the control parameters, which are strictly nonnegative. For

the coexistence equilibrium point  $E^* = (N^*, P^*, Z^*)$ , on increasing the value of  $a_1$  or  $c_1$ , we observe the sequence cold spots  $\rightarrow$  stripe–spots mixtures  $\rightarrow$  stripes  $\rightarrow$  hot stripe–spots mixtures  $\rightarrow$  hot spots  $\rightarrow$  chaotic wave patterns. This demonstrates that, in an ecological model, different ingestion rate  $a_1$  or mortality rate  $c_1$  of intermediate predator may play essentially different roles in developing spatial patterns. The ingestion rate and mortality rate of intermediate predator can enhance the oscillation of the species' density and form large clusters in space. The two-dimensional spatial patterns may indicate the vital role of phase transience regimes in the spatiotemporal organization of the predation food chain model.

The methods and results in the present paper may enrich research into pattern formation in the food chain model with diffusion in ecosystems.

**Acknowledgments** The author would like to express her gratitude to the editor and referees for their careful reading of the paper and a number of excellent criticisms and suggestions.

## References

- Baurmann, M., Gross, T., Feudel, U.: Instabilities in spatially extended predator–prey systems: spatio-temporal patterns in the neighborhood of Turing–Hopf bifurcations. *J. Theor. Biol.* **245**(2), 220–229 (2007)
- Beretta, E., Kuang, Y.: Global analyses in some delayed ratio-dependent predator–prey systems. *Nonlinear Anal. Theory Methods Appl.* **32**(3), 381–408 (1998)
- Berryman, A.: The origins and evolution of predator–prey theory. *Ecology* **73**(5), 1530–1535 (1992)
- Biktashev, V., Brindley, J., Holden, A., Tsyganov, M.: Pursuit–evasion predator–prey waves in two spatial dimensions. *Chaos* **14**(4), 988–995 (2004)
- Boer, M., Kooi, B., Kooijman, S.: Homoclinic and heteroclinic orbits to a cycle in a tri-trophic food chain. *J. Math. Biol.* **39**(1), 19–38 (1999)
- Camara, B.: Food web complexity analysis: effects of ecosystem changes. *Nonlinear Dyn.* **73**(3), 1783–1794 (2013)
- Cantrell, R., Cosner, C.: *Spatial Ecology Via Reaction–Diffusion Equations*. Wiley, New York (2003)
- Faithfull, C., Huss, M., Vrede, T., Bergström, A.: Bottom-up carbon subsidies and top-down predation pressure interact to affect aquatic food web structure. *Oikos* **120**(2), 311–320 (2011)
- Garvie, M.: Finite-difference schemes for reaction–diffusion equations modeling predator–prey interactions in MATLAB. *Bull. Math. Biol.* **69**(3), 931–956 (2007)
- Hou, H., Li, W.: Periodic solutions of a ratio-dependent food chain model with delays. *Taiwan. J. Math.* **8**(2), 211–222 (2004)
- Hsu, S., Hwang, T., Kuang, Y.: A ratio-dependent food chain model and its applications to biological control. *Math. Biosci.* **181**(1), 55–83 (2003)
- Klebanoff, A., Hastings, A.: Chaos in three species food chains. *J. Math. Biol.* **32**(5), 427–451 (1994)
- Ko, W., Ahn, I.: Analysis of ratio-dependent food chain model. *J. Math. Anal. Appl.* **335**(1), 498–523 (2007)
- Ko, W., Ahn, I.: Dynamics of a simple food chain model with a ratio-dependent functional response. *Nonlinear Anal. Real World Appl.* **12**, 1670–1680 (2011)
- Li, L., Jin, Z.: Pattern dynamics of a spatial predator–prey model with noise. *Nonlinear Dyn.* **67**(3), 1737–1744 (2012)
- Lin, Z., Pedersen, M.: Stability in a diffusive food-chain model with Michaelis–Menten functional response. *Nonlinear Anal. Theory Methods Appl.* **57**(3), 421–433 (2004)
- Liu, P., Xue, Y.: Spatiotemporal dynamics of a predator–prey model. *Nonlinear Dyn.* **69**(1–2), 71–77 (2012)
- Maini, P., Painter, K., Chau, H.: Spatial pattern formation in chemical and biological systems. *J. Chem. Soc. Faraday Trans.* **93**(20), 3601–3610 (1997)
- Maiorchi, D., dos Reis, S., de Aguiar, M.: Chaos and pattern formation in a spatial tritrophic food chain. *Ecol. Model.* **191**(2), 291–303 (2006)
- Malchow, H., Petrovskii, S., Venturino, E.: *Spatiotemporal Patterns in Ecology and Epidemiology—Theory, Models, and Simulation* (Mathematical and Computational Biology Series). CRC Press, Boca Raton, FL; Chapman and Hall, London (2008)
- Malchow, H., Radtke, B., Kallache, M., Medvinsky, A., Tikhonov, D., Petrovskii, S.: Spatio-temporal pattern formation in coupled models of plankton dynamics and fish school motion. *Nonlinear Anal. Real World Appl.* **1**(1), 53–67 (2000)
- Mulone, G., Straughan, B., Wang, W.: Stability of epidemic models with evolution. *Stud. Appl. Math.* **118**(2), 117–132 (2007)
- Murray, J.: *Mathematical Biology: I. An Introduction*, 3rd edn. Springer, New York (2002)
- Naji, R., Upadhyay, R., Rai, V.: Dynamical consequences of predator interference in a tri-trophic model food chain. *Nonlinear Anal. Real World Appl.* **11**(2), 809–818 (2010)
- Okubo, A., Levin, S.: *Diffusion and Ecological Problems: Modern Perspectives*, 2nd edn. Springer, New York (2001)
- Pang, P., Wang, M.: Qualitative analysis of a ratio-dependent predator–prey system with diffusion. *Proc. R. Soc. Edinb. A Math.* **133**(4), 919–942 (2003)
- Pathak, S., Maiti, A., Samanta, G.: Rich dynamics of a food chain model with Hassell–Varley type functional responses. *Appl. Math. Comput.* **208**(2), 303–317 (2009)
- Pearson, J.: Complex patterns in a simple system. *Science* **261**(5118), 189–192 (1993)
- Peng, R., Shi, J., Wang, M.: Stationary pattern of a ratio-dependent food chain model with diffusion. *SIAM J. Appl. Math.* **67**(5), 1479–1503 (2007)
- Rao, F., Wang, W., Li, Z.: Spatiotemporal complexity of a predator–prey system with the effect of noise and external forcing. *Chaos Solitons Fractals* **41**(4), 1634–1644 (2009)
- Rao, F.: Spatiotemporal pattern in a self- and cross-diffusive predation model with the Allee effect. *Discret. Dyn. Nat. Soc.* **2013**, 681641 (2013)

32. Shukla, J., Verma, S.: Effects of convective and dispersive interactions on the stability of two species. *Bull. Math. Biol.* **43**(5), 593–610 (1981)
33. Sun, G.: Pattern formation of an epidemic model with diffusion. *Nonlinear Dyn.* **69**(3), 1097–1104 (2012)
34. Turing, A.: The chemical basis of morphogenesis. *Philos. Trans. R. Soc. Lond. B* **237**(641), 37–72 (1952)
35. Upadhyay, R., Iyengar, S.: Effect of seasonality on the dynamics of 2 and 3 species prey–predator systems. *Nonlinear Anal. Real World Appl.* **6**(3), 509–530 (2005)
36. von Hardenberg, J., Meron, E., Shachak, M., Zarmi, Y.: Diversity of vegetation patterns and desertification. *Phys. Rev. Lett.* **87**, 198101 (2001)
37. Wang, Z., Hillen, T.: Classical solutions and pattern formation for a volume filling chemotaxis model. *Chaos* **17**, 037108 (2007)
38. Wang, Y., Wang, J.: Influence of prey refuge on predator–prey dynamics. *Nonlinear Dyn.* **67**(1), 191–201 (2012)
39. Wang, W., Lin, Y., Zhang, L., Rao, F., Tan, Y.: Complex patterns in a predator–prey model with self and cross-diffusion. *Commun. Nonlinear Sci. Numer. Simul.* **16**(4), 2006–2015 (2011)
40. Wang, W., Liu, Q., Jin, Z.: Spatiotemporal complexity of a ratio-dependent predator–prey system. *Phys. Rev. E* **75**, 051913 (2007)
41. Wang, B., Wang, A.L., Liu, Y.J., Liu, Z.H.: Analysis of a spatial predator–prey model with delay. *Nonlinear Dyn.* **62**(3), 601–608 (2010)
42. Xu, R., Chen, L.: Persistence and global stability for three-species ratio-dependent predator–prey system with time delays. *J. Syst. Sci. Complex.* **21**(2), 204–212 (2001)
43. Yang, L., Dolnik, M., Zhabotinsky, A., Epstein, I.: Pattern formation arising from interactions between Turing and wave instabilities. *J. Chem. Phys.* **117**, 7259 (2002)
44. Zeng, Z.: Dynamics of a non-autonomous ratio-dependent food chain model. *Appl. Math. Comput.* **215**, 1274–1287 (2009)
45. Zhou, J., Mu, C.: Positive solutions for a three-trophic food chain model with diffusion and Beddington–Deangelis functional response. *Nonlinear Anal. Real World Appl.* **12**(2), 902–917 (2011)